

Impact of the oceanic geothermal heat flux on a glacial ocean state

Maxime Ballarotta^{1,2}, Fabien Roquet^{3,2}, Saeed Falahat^{4,2}, Qiong Zhang^{1,2}, and Gurvan Madec^{5,6}

¹Department of Physical Geography, Stockholm University, Sweden

²Bolin Centre for Climate Research, Stockholm University, Sweden

³Department of Meteorology Stockholm University, Sweden

⁴Department of Environmental Science and Analytical Chemistry, Sweden

⁵Sorbonne Universités (UPMC, Univ. Paris 06)-CNRS-IRD-MNHN, LOCEAN Laboratory, Paris, France

⁶National Oceanography Centre, Southampton, United Kingdom

Correspondence to: M. Ballarotta (maxime.ballarotta@natgeo.su.se)

Abstract. The oceanic geothermal heating (OGH) has a significant impact on the present-day ocean state, but its role during glacial periods, when the ocean circulation and stratification were different from those of today, remains poorly known. In the present study, we analyzed the response of the glacial ocean to OGH, by comparing ocean simulations of the Last Glacial Maximum (LGM, ~21ka ago) including or not including geothermal heating. We found that applying the OGH warmed the Antarctic Bottom Waters (AABW) by ~0.4°C and increased the abyssal circulation by 15% to 30% north of 30°S in the deep Pacific and Atlantic basins. The geothermally heated deep waters were then advected toward the Southern Ocean where they upwelled to the surface due to the Ekman transport. The extra heat transport towards Antarctica acted to reduce the amount of sea ice contributing to the freshening of the whole AABW overturning cell. The global amount of salt being conserved, this bottom freshening induced a salinification of the North Atlantic and North Pacific surface and intermediate waters, contributing to the deepening of the North Atlantic Deep Water. This indirect mechanism is responsible for the largest observed warming, found in the North Atlantic deep western boundary current between 2,000 and 3,000 meters (up to 2°C). The characteristic time scale of the ocean response to the OGH corresponds to an advective time scale (associated with the overturning of the AABW cell) rather than a diffusive time scale. The OGH might facilitate the transition from a glacial to an inter-glacial state but its effect on the deep stratification seems insufficient to drive alone an abrupt climate change.

1 Introduction

20 The oceanic geothermal heating (OGH) is the heat flux through the sea floor which is generated by the internal heat content of the lithosphere. This flux is maximum near the oceanic ridges or underwater volcanic regions and is minimum ($\sim 50 \text{ mW.m}^{-2}$) in the abyssal plains (see e.g. Stein and Stein, 1992; Davies and Davies, 2010; Goutorbe et al., 2011).

25 The importance of the OGH as a heat source for the ocean system has long been controversial. Although the ocean is largely heated and thermally driven at the surface, several recent studies suggest that the OGH can also affect the ocean's dynamics and heat budget (Scott et al., 2001; Adcroft et al., 2001; Emile-Geay and Madec, 2009; Hofmann and Maqueda, 2009; Urakawa and Hasumi, 2009; Hieronymus and Nycander, 2012; Mashayek et al., 2013; de Lavergne et al., 2015). By applying a
30 spatially constant or variable heat flux in Ocean General Circulation Models (OGCMs) forced with the present day climate, it is shown that the OGH is a significant forcing that can weaken the stability of the water column, warm the bottom water and strengthen the abyssal thermohaline circulation ($\sim 5 \text{ Sv}$, $\text{Sv} = 10^6 \text{ m}^3 \cdot \text{s}^{-1}$).

35 Sparse observations suggest that the high oceanic heat fluxes associated with spreading centres favour bottom water thermo-dynamical changes on regional scale and centennial time scale (Detrick et al., 1974; Joyce et al., 1986; Hautala et al., 2005; Björk and Winsor, 2006). A recent study based on laboratory experiment further explored the role of the OGH. The study supports the strong effect of the OGH on the regional scale but minimises its impact on the thermohaline circulation and the
40 turbulent mixing (Zhou et al., 2014).

From a paleo-climate perspective, the abrupt release of potential energy due to the accumulation of OGH in the deep ocean is responsible for the rapid temperature variations observed in reconstructions of the last glacial cycles based on ice and sediment cores (Adkins et al., 2005). It is also
45 postulated that the OGH could have a large impact on the glacial overturning circulation and the deep water properties, such as the deep CO_2 storage (Adcroft et al., 2001). A climate simulation of the Neoproterozoic Era ($\sim 700 \text{ Ma}$ ago), when the Earth was entirely covered by ice (the so-called Snowball Earth hypothesis), reveals that the ocean is not stagnant and that the OGH may be a driver of its dynamic in decreasing the density of the abyssal waters, enhancing the convective vertical mixing and homogenising temperature and salinity in the water column (Ashkenazy et al., 2013, 2014).
50

To our knowledge, the impact of the OGH has not yet been investigated for more recent glacial climate period, such as the Last Glacial Maximum (LGM, $\sim 21 \text{ ka}$ ago), when the conditions were colder, the atmospheric CO_2 concentration was lower (Monnin et al., 2001) and the ocean stratification and deep circulation stronger than those found today (see e.g., Duplessy et al., 1988; Sarnthein
55

et al., 1994; Adkins et al., 2002; Adkins and Schrag, 2003; Curry, 2005; Lynch-Stieglitz et al., 2007; Otto-Bliesner et al., 2007). In the present study, we tested previously posed theories (e.g. Adkins et al., 2005) of the impact of the OGH on a glacial ocean state by using the forced LGM global configuration of Ballarotta et al. (2013) setup with realistic bathymetry and atmospheric forcing.

60 Here, we aim to 1) evaluate the impact of the OGH on the ocean circulation, in particular the North Atlantic and abyssal thermohaline circulation, the advective heat transport and the stratification; and 2) test whether the OGH could be a trigger of transition between glacial and interglacial climate. The paper is organised as follows: the ocean simulations are described in section 2; the impact of the OGH on the LGM simulated state is described in section 3; Results are discussed in section 4 and a

65 conclusion is given in section 5.

2 Model description

The NEMO-LIM2 model (Madec, 2008) was used to design the numerical experiments. The model configuration was similar to the experiment made by Emile-Geay and Madec (2009) in their study on the impact of the OGH in the present-day climate. NEMO solves the primitive equations discretised on a curvilinear horizontal mesh and was based in our study on a $2^\circ \times 2^\circ$ Mercator grid (namely

70 the ORCA2 global configuration). Within the tropics, the meridional resolution is increased up to 0.5° . The vertical dimension is discretised into 31 unevenly spaced depth levels (10 meters at the surface and 500 meters in the deep ocean). The LGM bathymetry is derived from the present-day bathymetry minus 120 meters, representative of the alteration of the sea level due to the freshwater

75 storage in the continental ice-sheets during the LGM. The vertical eddy viscosity and diffusivity coefficients required to model the vertical mixing were computed from the Turbulent Kinetic Energy (TKE) turbulent closure model (Gaspar et al., 1990; Blanke and Delecluse, 1993; Madec, 2008). The NEMO model uses the TEOS-10 equation of state (Roquet et al., 2015). The parameterisation of the mesoscale eddy-induced turbulence was established by the Gent and McWilliams (1990) formulation, which associates an eddy-induced velocity to the isoneutral diffusion. The ocean is coupled

80 to the Louvain-La-Neuve Ice Model LIM2 (Fichefet and Maqueda, 1997; Timmermann et al., 2005) which solves the thermodynamic growth and decay of the sea ice, the sea ice dynamics and its transport.

85 NEMO-LIM2 was initialised at rest and with the temperature, salinity and sea-ice fields averaged over the last 100 years of a 4,000 year long LGM experiment carried out with the MPI-OM coupled model (MPIOM LGM-W in Zhang et al. (2013)). The surface boundary conditions are computed using the CORE bulk formulae (Large and Yeager, 2004) and the atmospheric fields from a LGM quasi-equilibrated climate model experiment (Brandefelt and Otto-Bliesner, 2009). We took

90 the atmospheric forcing from Brandefelt and Otto-Bliesner (2009) because it corresponds to a quasi-

equilibrated state representative of an LGM state where the abyssal ocean is equilibrated to the LGM forcing. Note that no restoring sea surface salinity term was applied but the freshwater budget was constrained to have an instantaneous zero global mean value. A more exhaustive presentation of the experimental setup and boundary conditions can be found in Ballarotta et al. (2013). Although the
95 initial states used in Ballarotta et al. (2013) and in the present study originate from different models, they have similar structure: the temperature, salinity and sea-ice cover distribution are similar, in particular the deep saline waters in the abyss and the simulated large sea-ice cover.

For the present study, we designed a reference experiment (REF) without OGH at the sea floor. In
100 a second experiment (GH), spatially varying OGH fluxes were applied as the bottom boundary condition. Following Emile-Geay and Madec (2009), the OGH is computed from the age of the bedrock. We assumed that the OGH flux during the LGM was the same as today, since it is estimated from the age of the bedrocks expressed in million of years and that the LGM continental plate arrangement was similar to the modern day condition. The total energy input from the OGH forcing is 29.9 TW
105 ($TW = 10^{12}W$) and the mean value over the ocean is $\sim 88 \text{ mW}\cdot\text{m}^{-2}$. These values are slightly below the recent estimate of the OGH: the mean OGH value is $95.9 \text{ mW}\cdot\text{m}^{-2}$ and the total global heat flux is 30 to 31 TW (Davies and Davies, 2010; Davies, 2013). This OGH forcing modifies the heat content by changing the temperature trend in the model grid boxes just above the ocean floor.

110 For each configuration, NEMO was integrated for $\sim 14,000$ years and the analysis covered the last 100 model-years. At this stage of the integration, the ocean model was close to equilibrium. The annual mean model drift both in temperature and salinity was weak, with $< 0.006^\circ\text{C}/\text{century}$ ($< 0.003^\circ\text{C}/\text{century}$) below 500 meters and $< 0.09^\circ\text{C}/\text{century}$ ($< 0.08^\circ\text{C}/\text{century}$) in the upper 500 meters for REF (GH). The model drift in salinity was also weak for both GH and REF, with $<$
115 $0.004\text{PSU}/\text{century}$ below 500 meters and $< 0.012\text{PSU}/\text{century}$ in the upper layer.

3 Results

3.1 Impact of the geothermal heat flux on the stratification

The annual mean temperature trend induced by the OGH as a function of depth is shown in Figures 1a,b averaged over the Atlantic and the Indo-Pacific basins, respectively. In the GH experiment,
120 the Atlantic basin is $\sim 0.4^\circ\text{C}$ colder above 1,500 meters and gains heat below 1,500 meters with a maximum warming of $\sim 0.9^\circ\text{C}$ formed between 2,000 and 3,000 meters. In the Indo-Pacific basin, the upper 1,500 meters layer is $\sim 0.25^\circ\text{C}$ warmer, whereas the deep layer is up to 0.4°C warmer. In the Atlantic basin, the heat accumulation due to the OGH below 1,500 meters has a characteristic time scale of ~ 1600 years and reaches an asymptotic limit of 0.38°C (Figure 1c). In the Indo-Pacific
125 basin, the characteristic time scale is ~ 1200 years and the accumulated heat reaches an asymptotic

limit of 0.31°C . An equilibrium is reached after $\sim 10,000$ years.

The annual zonal mean temperature and salinity patterns in REF for the Atlantic and the Indo-Pacific basins are shown in Figures 2a,b,c,d. The deep ocean is filled with cold (near the freezing point of sea-water) and saline waters, which agrees with paleo-proxy reconstructions (Adkins et al., 2002; Adkins and Schrag, 2003) and the simulation by Brandefelt and Otto-Bliesner (2009). Relatively fresh and cold waters are found between 40°N and 90°N in the North Atlantic and North Pacific basins, due to the presence of sea ice.

The impact of the OGH on the zonal mean temperature and salinity patterns is shown in Figures 2e,f,g,h. The temperature differences are significant at all depths except in the upper 200 meters where the temperature variability is strong and mainly controlled by the atmospheric state. The North Atlantic cooling found in Figure 1 is mainly associated with colder surface water in the Nordic Seas (up to 0.7°C colder) and with the intrusion of colder Antarctic Intermediate Water (AAIW) in the South Atlantic basin (up to 1.3°C colder). The deep temperatures in the Atlantic Ocean are up to 1.3°C warmer, particularly between 1,500 and 3,000 meters in the deep western boundary current (Figure 3), and between 30°N and 45°N . In the Indo-Pacific basin, the layer below 1,500 meters is up to 0.4°C warmer and the surface layer is slightly colder (0.1°C colder) in the North Pacific basin and $\sim 0.3^{\circ}\text{C}$ warmer in the South Pacific. The salinity differences are significant at all depths and the patterns are relatively similar between the Atlantic and the Indo-Pacific basins: the Antarctic Bottom Water (AABW) is ~ 0.1 PSU fresher in GH than in REF whereas the upper layer is between 0.1 and 0.3 PSU saltier.

These differences in the temperature and salinity patterns modify the sea-water density (Figure 4). The AABW becomes less dense (the density decreases by $\sim 0.2 \text{ kg}\cdot\text{m}^{-3}$ in the Indo-Pacific, $0.3 \text{ kg}\cdot\text{m}^{-3}$ in the Atlantic) due to warming and freshening, whereas the density increases up to $0.3 \text{ kg}\cdot\text{m}^{-3}$ in the thermocline due to colder and more saline waters. The stratification (density gradient) is hence increased by $\sim 3\%$ near 2,250 meters and is reduced by $\sim 3\%$ near 3,250 meters (not shown).

3.2 Impact of the geothermal heat flux on the thermohaline circulation

Most paleo-climate studies investigate the thermohaline circulation in latitude-depth coordinates. A better description of the circulation is however found in latitude-density coordinates (Döös, 1994; Döös and Webb, 1994; Ballarotta et al., 2013) because fluid parcels are essentially constrained to move along density surface without doing work against gravitational force (McDougall, 1987). Ballarotta et al. (2014) have also shown that the strength of the glacial overturning strongly depends on the choice of coordinate system. Therefore, we present hereafter the meridional overturning circulation (MOC) in latitude-density coordinates, more precisely σ_4 (i.e., referenced to 4,000 meters),

in order to better capture and compare the abyssal circulation. Because the OGH affects the ocean's density structure, subtracting the streamfunctions in latitude-density coordinates is meaningless. It is however possible to identify the maximum of the AABW transport at each latitude, as well as
165 the density where the waters are formed. The MOC in latitude-depth coordinates is presented and discussed in the Appendix A for the reader who is not familiar with the MOC in latitude-density coordinates.

The annual mean residual (Eulerian mean + eddy induced velocities) MOC in latitude-density
170 coordinates is shown in Figures 5, for REF and GH. In the Southern Ocean, relatively dense waters ($\sigma_4 > 46.2 \text{ kg.m}^{-3}$) are formed between 60°S and 80°S . These waters are then transported almost adiabatically up to 40°N . The OGH intensifies the AABW cell by 15%-30% (from 20.5 Sv in REF to 23.4 Sv in GH in the Southern Ocean, 3.0 Sv to 3.7 Sv in the Atlantic basin, 6.3 Sv to 8.4 Sv in the Indo-Pacific basin) and shifts the maximum overturning towards lighter density classes (from
175 $\sigma_4 \sim 47.8 \text{ kg.m}^{-3}$ to $\sigma_4 \sim 47.6 \text{ kg.m}^{-3}$). The transport associated with the North Atlantic Deep Water (NADW) is ~ 4 Sv stronger in GH than in REF along the $46.5\text{-}46.7 \text{ kg.m}^{-3}$ isopycnals and the maximum of the North Atlantic overturning is 11% larger in GH (17.2 Sv) than in REF (15.4 Sv). The MOC in latitude-density coordinates also shows that the NADW is $\approx 0.1 \text{ kg.m}^{-3}$ denser in GH than in REF. Associated with it, the volume of the AABW in the Atlantic basin is eroded by $\sim 15\%$
180 in GH than in REF after 6,000 model years (Figure 6) when the layer below 1,500 meters is warmed by $\sim 0.3^\circ\text{C}$. In the Indo-Pacific basin, the volume of the AABW is only slightly larger (0.3%).

3.3 Impact on the northward heat transport

The annual mean residual (computed from Eulerian mean + eddy induced velocities) northward heat transport (in $\text{PW} = 10^{15}$ Watts) for the Global Ocean, the Atlantic basin and the Indo-Pacific basin in
185 REF is shown in Figure 7. In the Indo-Pacific basin, the heat transport reaches a maxima of 1 PW and 2 PW at 14°N and 14°S , respectively, and is directed northward in the northern hemisphere, and southward in the southern hemisphere. In the Atlantic basin, the heat transport is directed towards the North pole at all latitude and is maximum near 22°N (~ 0.9 PW). In the Southern ocean, the heat transport is less than 0.5 PW and directed towards Antarctica. The impact of the OGH on the
190 northward heat transport is statistically significant (based on a t-test, p-value less than 5%) in the Atlantic and Southern oceans. The AABW in the Indo-Pacific basin gains geothermal heat when it spreads northward. Most of this heat ($\sim 0.03\text{PW}$) is exported to the Southern Ocean surface where it diverges towards Antarctica (~ 0.02 PW) and towards the South Atlantic Ocean (~ 0.05 PW) near 50°S . The geothermal heat transported towards Antarctica then participates in the relative freshening
195 of the Southern Ocean surface water. The geothermal heat in the South Atlantic is transported northward and reaches a maximum of ~ 0.12 PW near 40°N , where the maximum mixed layer depths are found.

3.4 Intermediate summary and Impact on the North Atlantic deep convection

Our results suggest that the impact of the OGH on the glacial ocean stratification and thermohaline
200 circulation is significant. The OGH warms the AABW by $\sim 0.4^\circ\text{C}$ and increases the abyssal circula-
tion between 15% and 30% north of 30°S in the deep Pacific and Atlantic basins. The geothermally
heated deep waters are advected by the deep overturning cell and upwell at the Southern Ocean sur-
face. When reaching the Southern Ocean surface, these waters diverge near 50°S towards Antarctica
and towards the North Atlantic basin, due to the Ekman transport. The transport towards Antarctica
205 contributes to the freshening of the surface waters. As a result, the shelf waters that contribute to
the formation of AABW become fresher and the newly formed AABW becomes less saline. Due
to the global salt conservation, the freshening of the AABW is compensated by more saline sur-
face waters in the North Atlantic and North Pacific ($\sim 0.2\text{PSU}$ saltier), favouring the densification
and the deepening of the NADW. The largest warming is hence found in the North Atlantic deep
210 western boundary current between 2,000 and 3,000 meters due to the deepening of the thermocline.
Consequently, the volume of AABW is reduced by 15% in the Atlantic basin. We found that this
mechanism is relatively fast and has a characteristic time scale of $\sim 1,500$ years. It corresponds
mainly to an advective time scale (associated with the dynamics of the AABW) rather than a diffu-
sive time scale.

215

4 Discussion

The $\sim 0.4^\circ\text{C}$ warming of the abyssal ocean due to OGH is similar to the results found in simula-
tions of the present-day climate (Adcroft et al., 2001; Emile-Geay and Madec, 2009; Hofmann and
Maqueda, 2009). However, the largest temperature difference is found between 1,500 and 3,000 me-
220 ters in the Atlantic basin due to the deepening of the thermocline. This latest result coincides with
Hofmann and Maqueda (2009) in their present-day climate simulations where the North Atlantic
deep western boundary current warms between 0.9°C and 1.5°C , but it contrasts from the solution
found in the simulations from Adcroft et al. (2001) and Emile-Geay and Madec (2009) where the
largest warming takes place in North Pacific below 3,000 meters depth. The mechanism, explained
225 above, is compatible with the results found in Hofmann and Maqueda (2009). Both in our study and
in Hofmann and Maqueda (2009), and in opposition to Emile-Geay and Madec (2009) and other
studies, the ocean surface salinity is not relaxed towards a climatology. Therefore, the warming of
the abyssal waters contributes to freshening of the Southern Ocean surface waters via the advec-
tion of heat. The large formation of AABW contributes to fresher abyssal waters. Due to the closed
230 freshwater budget and no restoring term in the sea surface salinity in the model, the Southern Ocean
freshwater supply is counter-balanced by the densification of the surface waters becoming more
saline in the North Atlantic and Pacific Ocean. As a result, the AMOC is reinvigorated by the in-

creased surface salinity.

235 Turbulent mixing can also have an impact on the results. In the present study, we followed standard
practice for modelling mixing bounded with a minimum background mixing level. We are aware that
the mixing in our simulations might not be completely realistic for the LGM. In particular, the mix-
ing during the LGM was probably larger than today due to the emerged continental plateaus which
allow energy dissipation (Schmittner et al., 2015). As a result, larger energy in the mixing was prob-
240 ably supplied in the ocean interior, which contributes to erode the stratification more easily. Based
on the study of Emile-Geay and Madec (2009), our abyssal overturning will be larger in a context
of larger mixing. Our equilibrated state would thus be reached more quickly due to the increased
amount of energy dissipation, although we do not expect a qualitative change in our results. The
uncertainty due to the mixing and its variations through time is probably not larger than the overall
245 uncertainty on the surface forcing fields or on geothermal heating.

We found that the maximum of the AMOC is $\sim 11-15\%$ larger in GH than in REF, which is similar
to the anomaly found in simulation of the present-day climate (Hofmann and Maqueda, 2009). This
value may be considered as relatively important in light of the estimation made for the future climate
250 scenarios (an average reduction of 25% in Meehl et al. (2007) or on short time scale. However, it is
relatively weak compared to the variation of the AMOC on climate time scales, such as the 75% re-
duction with respect to LGM period during Heinrich stadial 1 ($\sim 15-18.5$ ka ago), the 45% reduction
during the Younger Dryas stadial (~ 12 ka ago) (Ritz et al., 2013), or the values found in fresh water
hosing experiments under LGM conditions ($> 20\%$ reduction in Kageyama et al. (2013)). In these
255 experiments, the AMOC changes are linked with surface processes, such as the freshwater discharge
(Heinrich, 1988; Hemming, 2004) which have a stronger and faster impact on the thermohaline cir-
culation than the processes induced by the OGH.

Similar to Adcroft et al. (2001) and Emile-Geay and Madec (2009), we found that the impact of
260 the OGH on the northward heat transport is weak ($\sim 10\%$) but non-negligible, particularly in the
Atlantic Ocean and in the polar regions as a result of the large scale advection of the abyssal heat
content. We found that the alteration of the ocean heat transport induced by the OGH in the North
Atlantic (~ 0.1 PW) is ~ 3 times larger than the total energy input provided by OGH (0.03 PW). How-
ever, the Southern Ocean Ekman transport prevents the accumulation of OGH in the abyssal ocean.
265 For a salinity gradient of ~ 1 PSU, a temperature gradient of $\sim 3^\circ\text{C}$ would be required to destabilise
the water column (see Appendix B). In the present study, the OGH warms by $\sim 0.4^\circ\text{C}$. Therefore the
OGH alone is probably not sufficient to destabilise the water column. Yet, OGH may facilitate the
transition from a glacial to an inter-glacial state by reducing the volume of saline abyssal waters by
 $\sim 15\%$ and reinvigorating the North Atlantic overturning by $\sim 10\%$, but OGH alone could not cause

270 abrupt climate changes.

5 Conclusions

In the present study, we investigated the response of the ocean to the geothermal heat flux during a glacial period, such as the LGM, when the ocean circulation and stratification were different from
275 today, and tested previously posed theories (Adkins et al., 2005) in a global ocean/ice model with realistic bathymetry. We found that the heat flux at the sea floor is a significant forcing of the deep ocean and the global thermohaline circulation. The Antarctic Bottom Water transports geothermally heated waters from the Indo-Pacific to the North Atlantic basin, indirectly favouring the deep convection in the North Atlantic and contributing to the deepening of North Atlantic Deep Water.

280

The deep ocean circulation and the OGH hence may speed up the transition from glacial to interglacial ocean state by reducing the volume of saline abyssal waters and reinvigorating the North Atlantic overturning. However, a new steady-state is achieved only a few thousands year after OGH is applied wherein the deep stratification, albeit weakened, remains extremely stable due to the strong
285 salinity gradient. We thus find it unlikely that abrupt climate changes could be triggered by the action of OGH alone during the LGM period. However, the OGH should contribute significantly in the transition between glacial and inter-glacial ocean states. The OGH has a strong effect on the ventilation of the abyssal ocean and might modulate the time scale of the overturning, and in turn, the rate of CO₂ release from the deep ocean to the atmosphere.

290

Our results are based on a forced (i.e. prescribed atmospheric conditions) ocean simulation of the LGM period. It does not account for possible ocean feedbacks on the atmosphere. Sensitivity studies with fully coupled ocean-atmosphere simulations would be useful to assess the impact of the OGH on the global climate system.

295 **Appendix A: Impact of the geothermal heat flux on the thermohaline circulation in latitude-depth coordinates**

In this section, we present the annual mean residual (Eulerian mean + eddy induced velocities) meridional overturning circulation (MOC) in latitude-depth coordinates (Figure 8a,b). The structure of the LGM thermohaline circulation agrees with the recent findings derived from multiple paleo-
300 proxies (Curry, 2005; Marchitto and Broecker, 2006; Lynch-Stieglitz et al., 2007; Evans and Hall, 2008; Tagliabue et al., 2009; Gherardi et al., 2009; Lippold et al., 2012; Adkins, 2013). The circulation representative of the North Atlantic Deep Water (NADW) in the upper 2,000 meters has a maximum transport of ~ 17 Sv at 900 meters depth near 35°N. It is slightly stronger and shallower

than in present-day simulations with same NEMO-ORCA2 model (Emile-Geay and Madec, 2009; 305 Lecointre, 2009; Brodeau et al., 2010), due to a larger intrusion of the AABW in the Atlantic basin.

The difference in the MOC between GH and REF is shown in Figure 8c,d for the Atlantic and Indo-Pacific basins. The impact of the OGH on the thermohaline circulation is statistically significant (based on a t-test, p-value less than 5%) in the Atlantic basin, in the Southern Ocean, in the 310 Arctic basin below 1,000 meters and in the Indo-Pacific basin below 3,000 meters. The volume transport in the downwelling branch and the deep current of the NADW is up to 5.6 Sv larger. It is mainly associated with the deepening of the NADW in the GH experiment. The maximum of the AMOC is $\sim 15\%$ larger in GH (20 Sv) than in REF (17 Sv). In the Southern Ocean, the volume transport is ~ 4 Sv larger in upwelling branch of the Deacon Cell, between 34° and 60° S. Note that the Deacon Cell 315 is fictitious and mainly appears in latitude-depth coordinates. The Southern Ocean overturning circulation is better described in latitude-density coordinates than in latitude-depth coordinates (Döös, 1994; Döös and Webb, 1994; Ballarotta et al., 2013), because it removes the fictitious Deacon Cell. The volume transport is ~ 4.1 Sv larger in the deep AABW cell between 45° S and 25° S and near Antarctica. In the North Atlantic and North Pacific, the volume transport in the AABW is between 1 320 and 2 Sv larger.

Appendix B: Ratio between the thermal expansion coefficient (α) and the saline contraction coefficient (β)

The ratio between the thermal expansion coefficient (α) and the saline contraction coefficient (β) is 325 $< \frac{1}{3} \text{ PSU} \cdot ^\circ\text{C}^{-1}$ in our simulation. It corresponds to the compensation of the variation of potential temperature due to changes of salinity (McDougall, 1987). Hence, for a salinity gradient of $\sim 1 \text{ PSU}$, a temperature gradient of minimum $\sim 3^\circ\text{C}$ would be required to destabilise the water column by mixing processes. In the present study, we found that the OGH warms the deep ocean by only 0.4°C . Therefore the OGH alone is not sufficient to abruptly destabilise the water column.

330 *Acknowledgements.* The authors acknowledge the National Supercomputer Centre at Linköping University (Sweden) for providing the computational resources to run the model. The simulations have been run on the Triolith super-computer (<https://www.nsc.liu.se/systems/triolith/>). Many thanks to Laurent Brodeau for installing the NEMO model on the Triolith platform.

References

- 335 Adcroft, A., Scott, J.R., and Marotzke, J.: Impact of geothermal heating on the global ocean circulation, *Geophysical Research letter*, 28, 1735–1738, doi: 10.1029/2000GL012182, 2001
- Adkins, J.F., McIntyre, K., and Schrag, D.P.: The Salinity, Temperature, and $\delta_{18}\text{O}$ of the Glacial Deep Ocean, *Science*, 298, 1769–1773, doi: 10.1126/science.1076252, 2002
- Adkins, J.F., and Schrag, D.P.: Reconstructing Last Glacial Maximum bottom water salinities from deep-sea sediment pore fluid profiles, *Earth and Planetary Science Letters*, 216, 109–123, doi: 10.1016/S0012-821X(03)00502-8, 2003
- 340 Adkins, J.F., Ingersoll, A., and Pasquero, C.: Rapid climate change and conditional instability of the glacial deep ocean from the thermobaric effect and geothermal heating, *Quaternary Science Reviews*, 24, 581–594, doi: 10.1016/j.quascirev.2004.11.005, 2005
- 345 Adkins, J.F.: The role of deep ocean circulation in setting glacial climates, *Paleoceanography*, 28, 539–561, doi:10.1002/palo.20046, 2013
- Ahn J., and Brook, E.J.: Atmospheric CO_2 and Climate on Millennial Time Scales During the Last Glacial Period, *Science*, 322, 83–85, doi: 10.1126/science.1160832, 2008
- Anderson, R.F., Ali, S., Bradtmiller, L.I., Nielsen, S.H.H., Fleisher, M.Q., Anderson, B.E., and Burckle, L.H.: 350 Wind-driven upwelling in the Southern Ocean and the deglacial rise in atmospheric CO_2 . *Science*, 323, 1443–1448, doi: 10.1126/science.1167441, 2009
- Ashkenazy, Y., Gildor, H., Losch, M., Macdonald, F. A., Schrag, D.P., and Tziperman, E.: Dynamics of a Snowball Earth ocean, *Nature*, 495, 90–93, doi:10.1038/nature11894, 2013
- Ashkenazy, Y., Gildor, H., Losch, M., and Tziperman, E.: Ocean Circulation under Globally Glaciated Snowball 355 Earth Conditions: Steady-State Solutions. *J. Phys. Oceanogr.*, 44, 24–43, doi: <http://dx.doi.org/10.1175/JPO-D-13-086.1>, 2014
- Ballarotta, M., Brodeau, L., Brandefelt, J., Lundberg, P., and Döös, K.: Last Glacial Maximum world ocean simulations at eddy-permitting and coarse resolutions: do eddies contribute to a better consistency between models and palaeoproxies?, *Clim. Past*, 9, 2669–2686, doi:10.5194/cp-9-2669-2013, 2013
- 360 Ballarotta, M., Drijfhout, S., Kuhlbrodt, T., and Döös, K.: The residual circulation of the Southern Ocean: Which spatio-temporal scales are needed?, *Ocean Modelling*, 64, 46–55, <http://dx.doi.org/10.1016/j.ocemod.2013.01.005>, 2013
- Ballarotta, M., Falahat, F., Brodeau, L. and Döös, K.: On the glacial and interglacial thermohaline circulation and the associated transports of heat and freshwater, *Ocean Sci.*, 10, 907–921, doi:10.5194/os-10-907-2014, 365 2014
- Björk, G., and Winsor, P.: The deep waters of the Eurasian Basin, Arctic Ocean: Geothermal heat flow, mixing and renewal, *Deep Sea Research Part I: Oceanographic Research Papers*, 53, 1253–1271, doi:10.1016/j.dsr.2006.05.006, 2006
- Blanke, B., and Delecluse, P.: Low frequency variability of the tropical atlantic ocean simulated by a general 370 circulation model with mixed layer physics. *J. Phys. Oceanogr.*, 23, 1363–1388, 1993
- Brandefelt J., and Otto-Bliesner B.L.: Equilibration and variability in a Last Glacial Maximum climate simulation with CCSM3, *Geophys. Res. Lett.*, 36, 1–5, doi:10.1029/2009GL040364, 2009

- Brodeau, L., Barnier, B., Treguier, A.-M., Penduff, T., and Gulev, S.: An ERA40-based atmospheric forcing for global ocean circulation models, *Ocean Modell.*, 31, 88–104, doi:10.1016/j.ocemod.2009.10.005, 2010
- 375 Curry, W. B.: Glacial water mass geometry and the distribution of $\delta_1^3\text{C}$ of ^{14}C in the western Atlantic Ocean, *Paleoceanography*, 20, 1–13, doi:10.1029/2004PA001021, 2005
- Davies, J., and Davies D.: Earth's surface heat flux, *Solid Earth*, 1, 5–24. doi: 10.5194/se-1-5-2010, 2010
- Davies, J. : Global map of solid Earth surface heat flow, *G3*, 14 (10), 4608–4622, 2013
- de Lavergne, C., Madec, G., Le Sommer, J., George Nurser, A. J., Naveira Garabato, A.C.: On the consumption
380 of Antarctic Bottom Water in the abyssal ocean, *J. Phys. Oceanogr.*, 46, 635–661, doi: 10.1175/JPO-D-14-0201.1, 2015
- Detrick, R., Williams, D., Mudie, J., and Sclater, J.: The Galapagos Spreading Centre: Bottom-Water Temperatures and the Significance of Geothermal Heating, *Geophysical Journal International*, 38, 627–637. doi: 10.1111/j.1365-246X.1974.tb05433.x, 1974
- 385 Döös, K., 1994. Semianalytical simulation of the meridional cells in the Southern Ocean. *Journal of Physical Oceanography* 24, 1281–1293.
- Döös, K., Webb, D., 1994. The Deacon Cell and the other meridional cells of the Southern Ocean. *Journal of Physical Oceanography* 24, 429–442.
- Duplessy, J.C., Shackleton, N.J., Fairbanks, R.G., Labeyrie, L., Oppo, D., and Kallel N.: Deepwater source variations during the last climatic cycle and their impact on the global deepwater circulation. *Paleoceanography*,
390 3, 343–360, 1988
- Emile-Geay, J., and Madec G.: Geothermal heating, diapycnal mixing and the abyssal circulation, *Ocean Science*, 5, 203–207, doi:10.5194/os-5-203-2009, 2009
- Evans, H. K., and Hall, I. R.: Deepwater circulation on Blake Outer Ridge (western North Atlantic) during the Holocene, Younger Dryas, and Last Glacial Maximum, *Geochem. Geophys. Geosy.*, 9, Q03023, doi:10.1029/2007GC001771, 2008
- 395 Ferrari, R., M. Jansen, J. Adkins, A. Burke, A. Stewart and A. Thompson: Antarctic sea ice control on ocean circulation in present and glacial climates, *Proc. Nat. Acad. Sciences*, Vol. 111 , 8753-8758, doi: 10.1073/pnas.1323922111, 2014
- 400 Fichefet T., and Maqueda, M.A.M.: Sensitivity of a global sea ice model to the treatment of ice thermodynamics and dynamics, *J. Geophys. Res.*, 102, 12609–12646, doi:10.1029/97JC00480, 1997
- Gaspar P., and Grégoris Y., Lefevre J.-M.: A simple eddy kinetic energy model for simulations of the oceanic vertical mixing: Tests at station papa and long-term upper ocean study site, *J. Geophys. Res.*, 95, 16179–16193, doi:10.1029/JC095iC09p16179, 1990
- 405 Gent P., and McWilliams J. Isopycnal mixing in Ocean Circulation models, *J. Phys. Oceanogr.*, 20, 150–155, Climatic impacts of fresh water hosing under Last Glacial Maximum conditions: a multi-model study, doi:10.1175/1520-0485(1990)020<0150:IMIOCM>2.0.CO;2, 1990
- Gherardi, J. M., Labeyrie, L., Nave, S., Francois, R., Mc-Manus, J. F., and Cortijo, E.: Glacial-interglacial circulation changes inferred from 231 Pa / 230 Th sedimentary record in the North Atlantic region, *Paleoceanography*, 24, 1–14, doi:10.1029/2008PA001696, 2009
- 410 Goutorbe, B., Poort, J., Lucazeau, F. and Raillard, S.: Global heat flow trends resolved from multiple geological and geophysical proxies, *Geophys. J. Int.*, 187, 1405–1419, doi: 10.1111/j.1365-246X.2011.05228.x, 2011

- Hautala S.L., Johnson H.P., Bjorklund T., (2005), Geothermal heating and the properties of bottom water in Cascadia Basin, *Geophysical Research Letters*, 32, L06608, doi: 10.1029/2004GL022342. issn: 0094-8276.
- 415 Heinrich, H.: Origin and consequences of cyclic ice rafting in the northeast Atlantic Ocean during the past 130,000 years, *Quaternary Res.*, 29: 142–152. doi:10.1016/0033-5894(88)90057-9, 1988
- Hemming, S.R.: Heinrich events: Massive late Pleistocene detritus layers of the North Atlantic and their global climate imprint. *Reviews of Geophysics*, 42, RG1005, DOI: 10.1029/2003RG000128, 2004
- Hieronymus M., and Nycander J.: The budgets of heat and salinity in NEMO, *Ocean Modelling*, 67, 28–38, 420 doi: 10.1016/j.ocemod.2013.03.006, 2012
- Hofmann M. and Maqueda M.: Geothermal heat flux and its influence on the oceanic abyssal circulation and radiocarbon distribution, *Geophysical Research letter*, 36, L03603, doi:10.1029/2008GL036078, 2009
- Joyce, T.M., and Warren, B.A., and Talley, L. D.: The geothermal heating of the abyssal subarctic Pacific Ocean, *Deep-Sea Res.*, 33, 1003–1015, doi: 10.1016/0198-0149(86)90026-9, 1986
- 425 Kageyama M., Merkel, U., Otto-Bliesner, B., Prange, M., Abe-Ouchi, A., Lohmann, G., Ohgaito, R., Roche, D. M., Singarayer, J., Swingedouw, D. and Zhang, X.: Climatic impacts of fresh water hosing under Last Glacial Maximum conditions: a multi-model study, *Clim. Past*, 9, 935–953, doi:10.5194/cp-9-935-2013, 2013
- Large, W. G., and S. Yeager, S.: Diurnal to decadal global forcing for ocean and sea-ice models : the data sets and flux climatologies. NCAR Technical Note, NCAR/TN-460+STR, CGD Division of the National Center 430 for Atmospheric Research, 2004
- Lecointre A., (2009), Variabilité interannuelle à décennale en atlantique nord et mers nordiques: Etudes conjointe d'observations, simulations numériques et réanalyses. PhD thesis, Université Joseph Fourier–Grenoble 1
- Lippold, J., Luo, Y., Francois, R., Allen, S. E., Gherardi, J., Pichat, S., Hickey, B., and Schulz, H., (2012) Strength and geometry of the glacial Atlantic Meridional Overturning Circulation, *Nat. Geosci.*, 5, 813–816, 435 doi:10.1038/ngeo1608.
- Lynch-Stieglitz, J., Adkins, J. F., Curry, W. B., Dokken, T., Hall, I., Herguera, J. C., Hirschi, J., Ivanova, E., Kissel, C., Marchal, O., Marchitto, T. M., McCave, I. N., McManus, J. F., Mulitza, S., Ninnemann, U., Peeters, F., Yu, E. F., and Zahn, R., (2007), Atlantic meridional overturning circulation during the Last Glacial Maximum, *Science*, 316, 66–69, doi:10.1126/science.1137127.
- 440 Madec G., (2008), NEMO ocean engine, Note du Pôle de modélisation de l'Institut Pierre-Simon Laplace No. 27, Institut Pierre-Simon Laplace, Paris, France, 2008.
- Marchitto, T. M. and Broecker, W. S., (2006) Deep water mass geometry in the glacial Atlantic Ocean: A review of constraints from the paleonutrient proxy Cd/Ca, *Geochem. Geophys. Geosys.*, 7, Q12003, doi:10.1029/2006GC001323.
- 445 Mashayek, A., R. Ferrari, G. Vettoretti, and W. R. Peltier (2013), The role of the geothermal heat flux in driving the abyssal ocean circulation, *Geophys. Res. Lett.*, 40, 3144-3149, doi:10.1002/grl.50640.
- McDougall, T.J. (1987), Neutral density surface in the ocean: implications for modelling, *Geophys. Res. Lett.*, 14, 797-800, 10.1029/GL014i008p00797.
- Meehl, G.A., T.F. Stocker, W.D. Collins, P. Friedlingstein, A.T. Gaye, J.M. Gregory, A. Kitoh, R. Knutti, J.M. 450 Murphy, A. Noda, S.C.B. Raper, I.G. Watterson, A.J. Weaver and Z.-C. Zhao, (2007), Global Climate Projections. In: *Climate Change 2007: The Physical Science Basis. Contribution of Working Group I to the Fourth Assessment Report of the Intergovernmental Panel on Climate Change* [Solomon, S., D. Qin, M. Manning, Z.

- Chen, M. Marquis, K.B. Averyt, M. Tignor and H.L. Miller (eds.)). Cambridge University Press, Cambridge, United Kingdom and New York, NY, USA.
- 455 Monnin E., A. Indermühle, A. Daellenbach, J. Flueckiger, B. Stauffer, T. F. Stocker, D. Raynaud, J. M. Barnola (2001), Atmospheric CO₂ concentrations over the Last Glacial Termination, *Science*, 291, 112–114, doi: 10.1126/science.291.5501.112
- Otto-Bliesner, B. L., Hewitt, C. D., Marchitto, T. M., Brady, E. C., Abe-Ouchi, A., Crucifix, M., Murakami, S., and Weber, S. L., (2007), Last Glacial Maximum ocean thermohaline circulation: PMIP2 model intercomparisons and data constraints, *Geophys. Res. Lett.*, 34 1–6, doi:10.1029/2007GL029475.
- 460 Petit, J.R., Jouzel, J., Raynaud, D., Barkov, N.I., Barnola, J.-M., Basile, I., Bender, M., Chappellaz, J., Davis, M., Delaygue, G., Delmotte, M., Kotlyakov, V.M., Legrand, M., Lipenkov, V.Y., Lorius, C., Pepin, L., Ritz, C., Saltzman, E., and Stievenard, M.: Climate and atmospheric history of the past 420,000 years from the Vostok ice core, Antarctica. *Nature* 399: 429–436, 1999
- 465 Ritz, S.P., Stocker, T.F., Grimalt, J.O., Menviel, L., and Timmermann, A.: Estimated strength of the Atlantic overturning circulation during the last deglaciation. *Nat. Geosci.* 6, 208–212, 2013
- Roquet, F. and Madec, G. and McDougall, Trevor J. and Barker, Paul M.: Accurate polynomial expressions for the density and specific volume of seawater using the TEOS-10 standard. *Ocean Modelling* 90, 29–43, 2015
- Sarnthein, M., Winn, K., Jung, S.J.A., Duplessy, J.C., Labeyrie, L., Erlenkeuser, H., and Ganssen, G.: Changes
470 in east Atlantic deep-water circulation over the last 30,000 years – 8 time slice reconstructions. *Paleoceanography* 9, 209–267, 1994
- Schmittner, A., Green, J. A. M. and Wilmes, S.-B. : Glacial ocean over- turning intensified by tidal mixing in a global circulation model, *Geophys. Res. Lett.*, 42, doi:10.1002/2015GL063561, 2015
- Scott, J., Marotzke, J., and Adcroft, A.: Geothermal heating and its influence on the meridional overturning
475 circulation. *Journal of Geophysical Research*, 106(C12), 31141–31154, doi:10.1029/2000JC000532, 2001
- Siegenthaler, U., Stocker, T. F., Monnin, E., Lüthi, D., Schwander, J., Stauffer, B., Raynaud, D., Barnola, J.-M., Fischer, H., Masson-Delmotte, V., and Jouzel, J. (2005) Stable carbon cycle-climate relationship during the last Pleistocene, *Science*, 310, 1313– 1317, doi: 10.1126/science.1120130.
- Skinner L. C., S. Fallon, C. Waelbroeck, E. Michel, S. Barker, (2010), Ventilation of the Deep Southern Ocean
480 and Deglacial CO₂ Rise, *Science*, 328, 1147, doi: 10.1126/science.1183627.
- Stein C., and Stein S.: A model for the global variation in oceanic depth and heat flow with lithospheric age. *Nature*, 359, 123–129, doi: 10.1038/359123a0, 1992
- Tagliabue, A., Bopp, L., Roche, D. M., Bouttes, N., Dutay, J.-C., Alkama, R., Kageyama, M., Michel, E., and
485 Paillard, D.: Quantifying the roles of ocean circulation and biogeochemistry in governing ocean carbon-13 and atmospheric carbon dioxide at the last glacial maximum, *Clim. Past*, 5, 695–706, doi:10.5194/cp-5-695-2009, 2009
- Timmermann, R., Goosse, H., Madec, G., Fichet, T., Ethe, C., Dulière, V.: On the representation of high latitude processes in the ORCA-LIM global coupled sea ice-ocean model, *Ocean Modelling* 8, 175–201, doi:10.1016/j.ocemod.2003.12.009, 2005
- 490 Toggweiler, J.R., Russell, J.L., and Carson, S.R.: Midlatitude westerlies, atmospheric CO₂, and climate change during the ice ages. *Paleoceanography* 21, PA2005. doi:10.1029/2005PA001154, 2006

- Urakawa, L., and Hasumi, H.: A remote effect of geothermal heat on the global thermohaline circulation. *Journal of Geophysical Research*, 114, C07016, doi:10.1029/2008JC005192, 2009
- 495 Watson, A.J., and Garabato, A.C.N.: The role of Southern Ocean mixing and upwelling in glacial–interglacial atmospheric CO₂ change. *Tellus* 58B, 73–87, doi: 10.1111/j.1600-0889.2005.00167.x, 2006
- Worthington, L.: Genesis and Evolution of Water Masses, *Meteor. Mon.*, 8, 63–67, 1968.
- Zhang X., Lohmann G., Knorr G., and Xu X.: Different ocean states and transient characteristics in Last Glacial Maximum simulations and implications for deglaciation, *Climate of the Past*, 9, 2319–2333, doi:10.5194/cp-9-2319-2013, 2013
- 500 Zhou S., Qu L., Zhao X., and Wan W.: Laboratory simulation of the influence of geothermal heating on the interior ocean, *Acta Oceanologica Sinica*, 33, 25–31, doi: 10.1007/s13131-014-0512-8, 2014

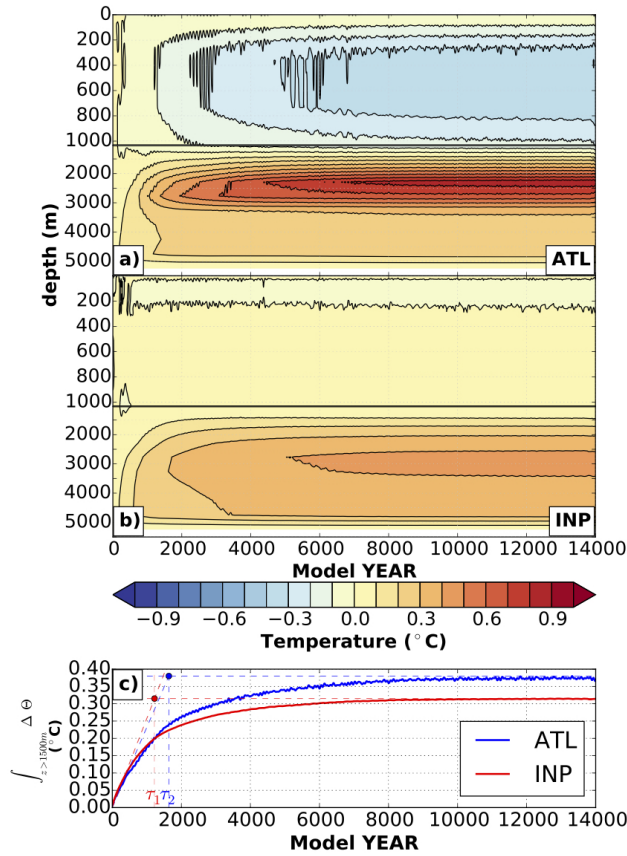


Figure 1. Annual mean potential temperature trend (in °C) induced by the geothermal heat forcing as a function of depth averaged in **a)** the Atlantic basin and **b)** the Indo-Pacific basin. Contour intervals are every 0.1 °C. Note the vertical scale is increased in the upper 1000 meters. **c)** Time-series of the mean temperature accumulation (in °C) due to the geothermal heat below 1,500 meters in the Atlantic and Indo-Pacific basins. $\tau_1 \sim 1200$ years and $\tau_2 \sim 1600$ years denote the characteristic time scale, i.e. the amount of time required for the response to reach $(1-1/e) \approx 63\%$ of the maximum heat accumulation, in the Indo-Pacific and the Atlantic basins

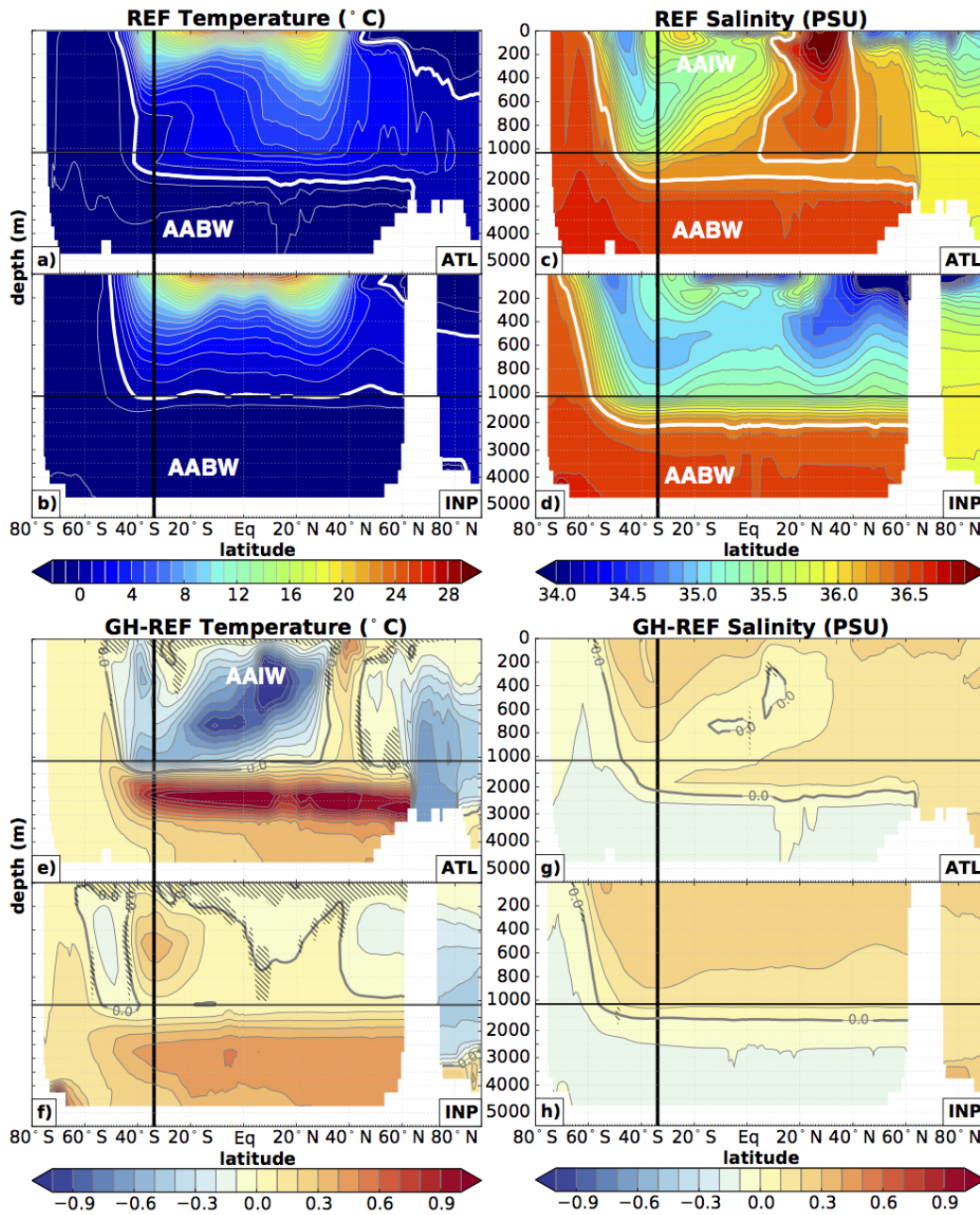


Figure 2. Annual zonal mean potential temperature patterns (in $^{\circ}\text{C}$) in the reference experiment (REF) for **a)** the Atlantic basin, **b)** the Indo-Pacific basin (Contour interval every 1°C , thick white contour is 0°C); salinity patterns (in PSU) in the reference experiment (REF) for **c)** the Atlantic basin, **d)** the Indo-Pacific basin (Contour interval every 0.1PSU , thick white contour is 36.3PSU); the temperature difference between REF and GH for **e)** the Atlantic basin, and **f)** the Indo-Pacific basin (Contour interval every 0.1°C , thick grey contour is 0°C); and salinity difference between REF and GH for **g)** the Atlantic basin, and **h)** the Indo-Pacific basin (Contour interval every 0.1PSU , thick white contour is 0PSU). The thick vertical black line shows the location of the Southern Ocean entrance at 34°S . Note the vertical scale is increased in the upper 1,000 meters. The patterns in each Southern Ocean sector are shown in each panel between 80°S and 34°S . The hatched regions represent the regions where the difference is insignificant at a 95% confidence level (based on a t-test). AABW: Antarctic Bottom Water, AAIW: Antarctic Intermediate Water

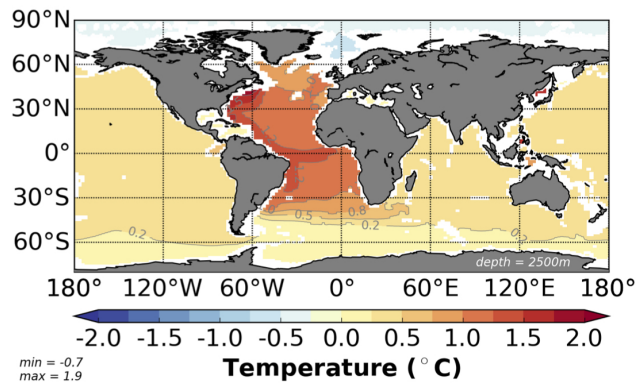


Figure 3. Map of the annual mean temperature difference (in °C) between GH and REF at 2,500 meters. Maximum and minimum values are denoted in the lower left corner. The largest warming is in the Atlantic deep western boundary current

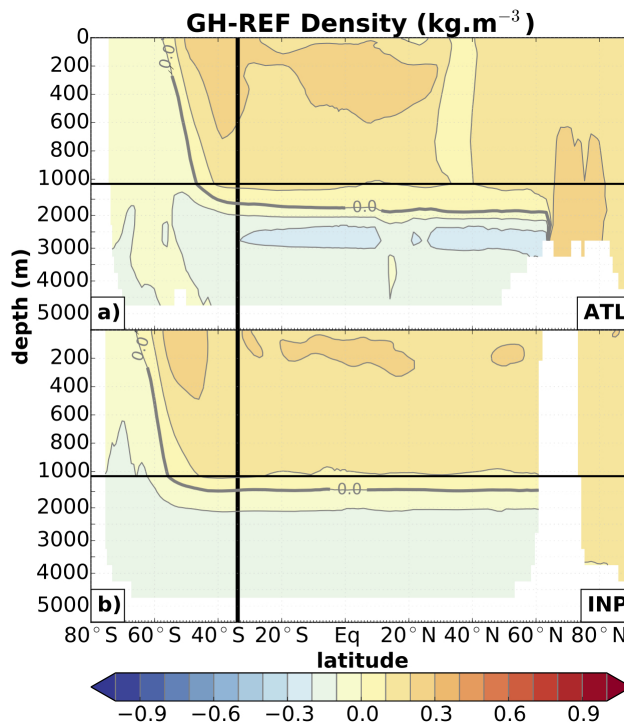


Figure 4. Difference in the annual mean and zonal mean potential density patterns (σ_4 in kg.m^{-3}) between REF and GH for **a)** the Atlantic basin, and **b)** the Indo-Pacific basin. Contour and scale same as in Fig. 2

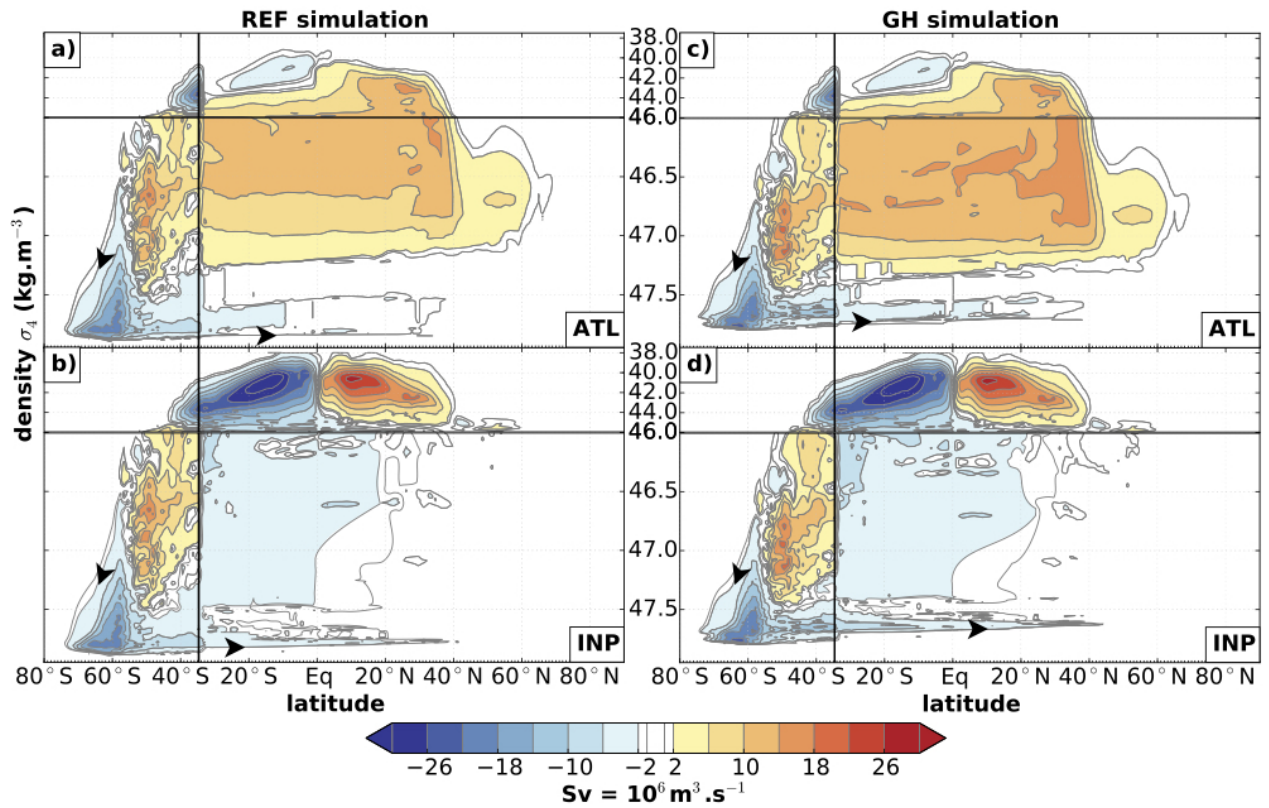


Figure 5. Annual mean density-binned residual (Eulerian + eddy-induced velocities) meridional overturning circulation (in Sv) in the experiment *without* geothermal heating (REF) for **a)** the Atlantic basin, and **b)** the Indo-Pacific basin; and in the experiment *with* geothermal heating (GH) for **c)** the Atlantic basin, and **d)** the Indo-Pacific basin. The thick black line shows the location of the Southern Ocean entrance at 34°S. The annual mean meridional overturning circulation in the Southern Ocean is shown in each panel between 80°S and 34°S. Positive (negative) contours represent clockwise (anti-clockwise) circulations. Contour interval is every 4Sv, and -1 and +1 Sv contours are added. Density bins intervals every 0.01kg.m^{-3} . Note the vertical scale is increased for $\sigma_4 > 46 \text{ kg.m}^{-3}$

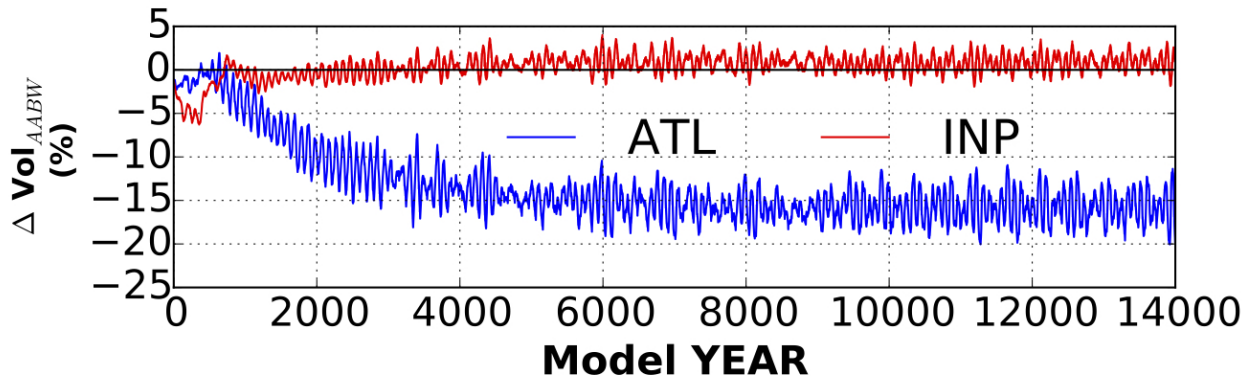


Figure 6. Time-series of the AABW volume variation (in %) in the Atlantic and Indo-Pacific basins. The AABW volume is computed as the volume of water below 2,000 m where the annual mean residual overturning circulation in latitude-depth coordinates is negative (Figure 8a,b). Note that the volume of the lower meridional circulation cell does not necessarily coincide with the volume occupied by Antarctic Bottom Water, because circulation boundaries do not necessarily match water-mass boundaries

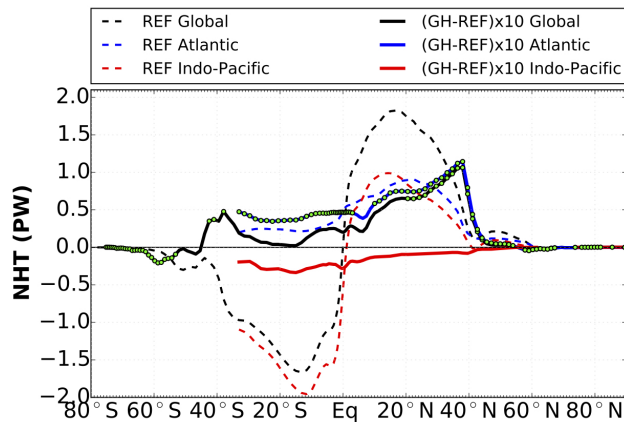


Figure 7. Annual mean residual (Eulerian mean + eddy-induced velocities) northward heat transport (in $\text{PW}=10^{15}$ Watts) in the Global Ocean, the Atlantic and the Indo-Pacific basins in the reference experiment (dashed line); and the difference between REF and GH in the annual mean northward heat transport (thick line). Note that the difference is magnified by a factor 10. The green dots show where the difference is significant at a 95% confidence level (based on a t-test)

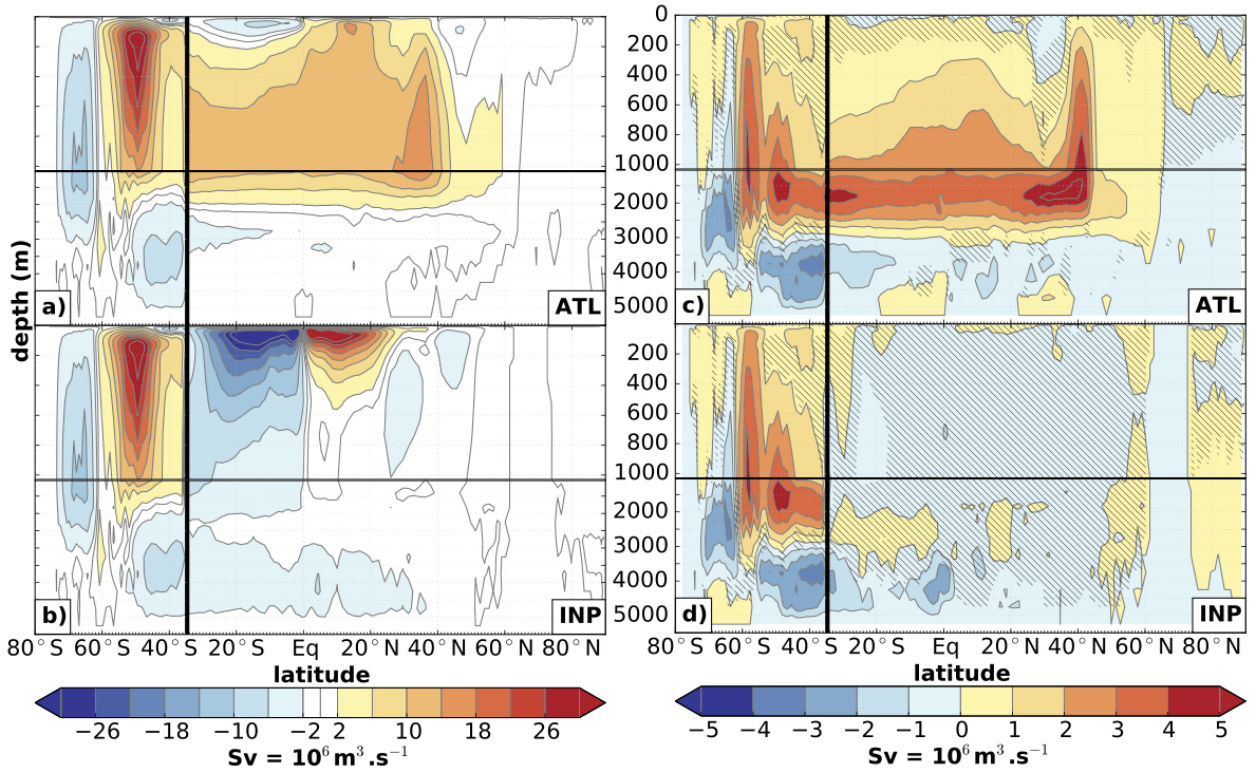


Figure 8. Annual mean residual (Eulerian mean + eddy-induced velocities) meridional overturning circulation in latitude-depth coordinates (in $Sv=10^6 m^3.s^{-1}$) in the reference experiment (REF) for **a)** the Atlantic basin, and **b)** the Indo-Pacific basin. Contour interval is every $4Sv$, and the $0 Sv$ contours is added. Positive (negative) values represent clockwise (counter-clockwise) circulation. Difference in the residual meridional overturning circulation between REF and GH for **c)** the Atlantic basin, and **d)** the Indo-Pacific basin. Contour interval is every $1Sv$. The annual mean meridional overturning circulation and the difference in the meridional overturning circulation in the Southern Ocean between GH and REF is shown $80^{\circ}S$ and $34^{\circ}S$. Note the vertical scale is increased in the upper 1,000 meters. The hatched regions represent the regions where the difference is insignificant at a 95% confidence level (based on a t-test)